Original Research

Accuracy of Phase-Contrast Flow Measurements in the Presence of Partial-Volume Effects[1]

Chao Tang, PhD • Duane D. Blatter, MD • Dennis L. Parker, PhD

The accuracy of volume flow rate measurements obtained with phase-contrast methods was assessed by means of computer simulation and in vitro experiments. Factors studied include (*a*) the partial-volume effect due to voxel dimensions relative to vessel dimensions and orientation and (*b*) intravoxel phase dispersion. It is shown that limited resolution (partial-volume effect) is the major obstacle to accurate flow measurement for both laminar and plug flow. The results show that at least 16 voxels must cover the cross section of the vessel lumen to obtain a measurement accuracy to within 10%. Measurement accuracy also greatly depends on the relative signal intensity of stationary tissue and is better for laminar flow than plug flow.

Index terms: Blood, flow dynamics, 57.12944 • Flow artifacts • Flow simulation • Model, mathematical • Phantoms • Phase imaging • Vascular studies

JMRI 1993; 3:377–385

Abbreviation: SR = saturation ratio.

[1] From the Departments of Medical Informatics (D.L.P.) and Physics (C.T.), University of Utah, 325 8th Ave, Salt Lake City, UT 84143; and the Department of Radiology, LDS Hospital, Salt Lake City, Utah (D.D.B.). Received March 23, 1992; revision requested June 23; final revision received and accepted September 9. **Address reprint requests to** D.L.P.

TWO BASIC PHYSICAL principles, time of flight and phase contrast, have been used to acquire flow images with great success in magnetic resonance (MR) imaging. Time of flight (1,2) uses the inflow of unsaturated spins for differentiation from stationary spins. Phase contrast (3,4) relies on the phase shift of spins moving along the direction of a bipolar velocity-encoding gradient for differentiation from stationary spins. Phase-contrast techniques have the added advantage that direct measurements of flow velocity and volume flow rate can be obtained (5,6).

In the present study, the accuracy and precision of phase-contrast flow measurements were assessed by means of computer simulation and in vitro experiments. In the simulations, both laminar and plug flow were assumed. We first review the principles of phase-contrast velocity imaging and discuss the factors that appear to affect the accuracy of quantitative phase-contrast flow measurements. These factors include (*a*) partial-volume effects due to voxel dimensions relative to vessel dimensions and orientation and (*b*) intravoxel phase dispersion. The effect of nonconstant flow (eg, pulsatile flow) is not considered here. However, the analysis should be relevant to a single frame in a gated study if the motion is periodic and higher-order-motion effects are negligible. Simulation studies and in vitro experiments are then presented. The results of the simulations and experiments show the extent to which partial-volume effects—which arise from partially occupied voxels at the boundary of the vessel—reduce measurement accuracy. Errors due to vessel angulation can be understood in terms of angle-dependent partial-volume effects.

• THEORY

Phase-contrast velocity imaging requires the application of a bipolar velocity-encoding gradient waveform, as shown in Figure 1. Such a flow-encoding gradient induces a phase shift in a moving element of tissue that is directly related to the component of tissue velocity in the direction of the encoding gradient. If the flow-encoding gradient is applied in the z direction, the phase for spins flowing with a constant velocity v_z in the z direction is given by

$$\phi_1 = k_1 v_z + \phi_0, \quad (1)$$

where ϕ_0 is the phase shift in the absence of flow and k_1 is the product of γ, the gyromagnetic ratio, and the first moment of the flow-encoding gradient, or

$$k_1 = \gamma \int tG(t)dt. \quad (2)$$

Similarly, the phase shift for a second flow-encoding gradient waveform can be expressed as

$$\phi_2 = k_2 v_z + \phi_0. \quad (3)$$

From Equations (1) and (3), we can obtain the z component of the velocity:

$$v_z = \frac{\phi_2 - \phi_1}{k_2 - k_1}. \quad (4)$$

The volume flow rate through a section perpendicular to the z axis is the surface integral

$$Q = \int v_z ds. \quad (5)$$

To avoid velocity aliasing, the extent of the range of the phase difference between the two acquisitions should be less than 2π (eg, between $-\pi$ and π). If we design the bipolar gradients to encode the same maximum velocity in both directions, we find that the encoding velocity v_{enc}, which corresponds to a phase difference of π for fixed velocity-encoding gradients, will be

$$v_{enc} = \frac{\pi}{k_2 - k_1}. \quad (6)$$

Motion in all three directions can be analyzed (7,8) with repeated sequences in which pairs of flow-encoding gradient waveforms are applied in each direction.

The above discussion applies to flow measurements with infinite resolution. In the realistic situation of finite resolution, both velocity dispersion and the mixture of stationary and flowing spins within a voxel (partial-volume effect) will result in velocity and flow measurement errors (9). Because of the resulting phase dispersion, velocity dispersion within a voxel can result in a signal loss or void and a subsequent error in flow measurement.

Partial-volume effects occur when the signal-generating components are not uniform within a voxel. Figure 2 shows two different tissues, represented by the shaded and unshaded area. Voxels such as *A*, which are occupied by more than one tissue, are called partially occupied voxels. If quantitation of a specific component is performed by adding the volume of voxels containing that component, an error will result owing to the uncertainty about whether to include or exclude these partially occupied voxels in the measurement. No such error would occur in voxels such as *B* and *C*, which are occupied by a single tissue type. For the purpose of this study, voxels totally occupied by flowing spins with or without velocity dispersion are not considered partially occupied voxels. We limit our analysis of the partial-volume effect to voxels that are only partially occupied by flowing spins. Although this is a more narrow definition of the effect, it allows us to consider phase dispersion due to velocity dispersion in laminar flow as a separate phenomenon.

We now derive the equations that describe the flow-dependent signal in each voxel by considering both

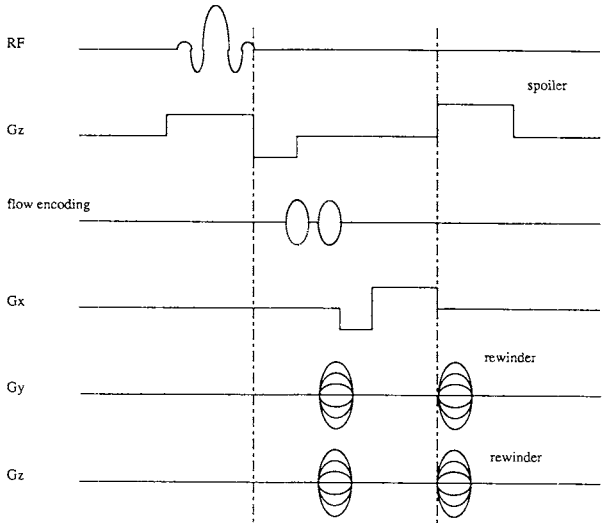

Figure 1. Radio-frequency (*RF*) and gradient waveforms for a three-dimensional phase-contrast pulse sequence. In the present study, the flow-encoding gradients were incorporated only in the section-select direction (z). If two-dimensional phase-contrast methods are used, the position phase-encoding gradient in the z direction (bottom line) is omitted.

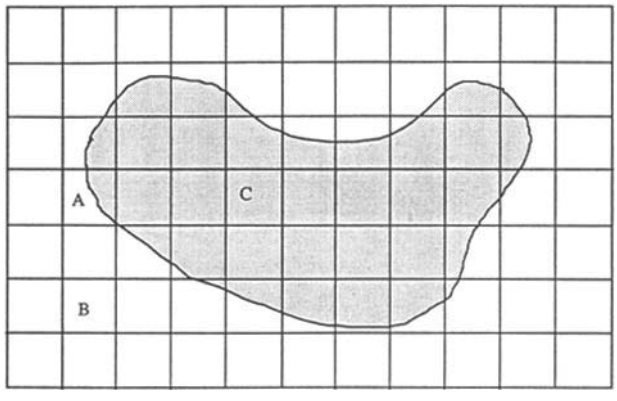

Figure 2. Schematic illustrates the partial-volume effect. Two different tissues are represented by the shaded and the unshaded areas. Voxels such as *B* and *C* include only one tissue. Voxels such as *A*, which are called partially occupied voxels, include more than one type of tissue.

phase dispersion and the partial-volume effect. Consider a voxel that is occupied by both stationary and flowing spins. Figure 3 shows how the partial-volume effect influences the velocity measurement, where Z_s is the voxel magnetization contribution from stationary spins. Z_{1v} and Z_{2v}, which are the voxel magnetization contributions from the flowing spins only, are obtained by using two different forms of velocity-encoding gradients:

$$Z_{1v} = \int \rho_{(v_z)} \exp(ik_1 v_z) dv_z, \quad (7)$$

$$Z_{2v} = \int \rho_{(v_z)} \exp(ik_2 v_z) dv_z, \quad (8)$$

where $\rho_{(v_z)}$ is the distribution of the z component of velocity inside one voxel.

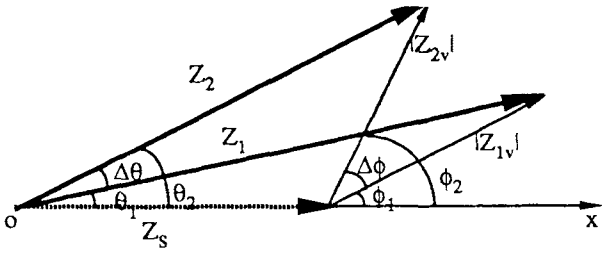

Figure 3. Magnetization vector obtained from two flow measurements. Z_1 and Z_2 are the total magnetization vectors for two flow measurements, respectively. Z_S (dotted line) is the magnetization of stationary spins. Z_{1v} and Z_{2v} are the magnetization vectors for flowing spins in the two acquisitions, respectively. $\Delta\theta$ is the measured phase shift. $\Delta\phi$ is the phase shift of flowing spins.

Z_{1v} and Z_{2v} represent the net magnetization of flowing spins. In general, the magnitudes of Z_{1v} and Z_{2v} will not be the same unless no velocity dispersion occurs in the voxel. In the case of plug flow, the velocity distribution $\rho_{(v_z)}$ will be a delta function and there will be no phase dispersion among the flowing spins. In the case of laminar flow, $\rho_{(v_z)}$ will not be a delta function. The phase dispersion of the flowing spins will vary with voxel size and position in the vessel. Note that we do not consider time-of-flight effects in these expressions. Because we are measuring the phase difference, there will be little, if any, error due to variation in signal strength for totally occupied voxels. The only substantial time-of-flight–related error will occur in the boundary voxels, and these will all experience essentially the same partial-saturation signal loss.

As shown in Figure 3, we define Z_1 and Z_2 to be the net magnetization within a voxel from both flowing spins and stationary spins for the first and second acquisition, respectively:

$$Z_1 = Z_{1v} + Z_s, \tag{9}$$

$$Z_2 = Z_{2v} + Z_s. \tag{10}$$

The magnitude of the voxel signal in the images from the two acquisitions is equal to $|Z_1|$ and $|Z_2|$, respectively. The phase shift difference between the two acquisitions can be expressed as

$$\Delta\theta = \theta_2 - \theta_1, \tag{11}$$

where

$$\theta_1 = \arctan\left[\frac{|Z_{1v}| \sin \phi_1}{|Z_{1v}| \cos \phi_1 + |Z_s|}\right], \tag{12}$$

$$\theta_2 = \arctan\left[\frac{|Z_{2v}| \sin \phi_2}{|Z_{2v}| \cos \phi_2 + |Z_s|}\right]. \tag{13}$$

For voxels in which there is no signal from stationary spins (ie, if Z_s is zero), $\Delta\theta$ is equal to $\Delta\phi$, where $\Delta\phi$ is defined as

$$\Delta\phi = \phi_2 - \phi_1. \tag{14}$$

For any voxel (*i*th voxel) that is totally occupied by flow of a single velocity, the velocity can be obtained by using Equations (4) and (6):

$$v_i = \frac{\Delta\theta}{\pi} v_{enc}. \tag{15}$$

If Δs is the voxel cross-sectional area perpendicular to the flow, the volume flow rate through the voxel is simply

$$Q_i = v_i \Delta s. \tag{16}$$

Although Equations (15) and (16) are valid only for uniform flow within a voxel, they are routinely applied in phase-contrast velocity measurements, even in the presence of velocity dispersion and partial-volume effects. If there is no stationary signal and no velocity dispersion in a partially occupied voxel, the volume flow rate of the voxel will be overestimated because the cross-sectional area is overestimated while the velocity of flowing spins is measured accurately.

The total measured volume flow rate Q_m through a tube is equal to the summation of all the voxel volume flow rates Q_i for the voxels that cover the cross section of the lumen of the tube:

$$Q_m = \sum_i Q_i. \tag{17}$$

The difference between the volume flow rate obtained by using Equation (17) and the true flow rate obtained by using Equation (5) is the phase-contrast flow measurement error.

It can be seen from Equations (11)–(13) that the accuracy of the measured volume flow rate Q_m obtained will depend on the flow type (laminar or plug) and the relative magnitudes of Z_{1v}, Z_{2v}, and Z_s. Because shifting the shaded region in Figure 2 will change the partition in a partially occupied volume, we expect that Q_m will also depend on the relative position between vessel and voxel grids.

When Z_s is not zero, the partial-volume effect results in compensating errors for the two terms included in Equation (16). The measured velocity v_i is usually less than the mean velocity of flowing spins within the voxel because the measured phase shift $\Delta\theta$ usually underestimates the velocity phase shift $\Delta\phi$, owing to the presence of stationary spins. On the other hand, the voxel cross-sectional area Δs is larger than the relative cross-sectional area of flowing spins in the voxel. The net error in volume flow measurement will depend on the relative magnitudes of the two compensating errors.

If resolution is increased, we expect that errors arising from partial-volume effects will diminish. Consider a round vessel residing in stationary tissue and images with resolution N. The number of voxels that cover the cross section of the vessel lumen is proportional to N^2. The number of voxels that are partially occupied is proportional to N. The relative error in flow measurement due to partial-volume effects will be proportional to $1/N$. The higher the resolution, the more accurate the flow measurement. This is verified by simulations and experiments.

Finally, if the vessel is at an angle α with respect to the direction of section selection and velocity encoding, the vessel cross-sectional area increases by $1/\cos \alpha$ and the velocity measured will decrease by

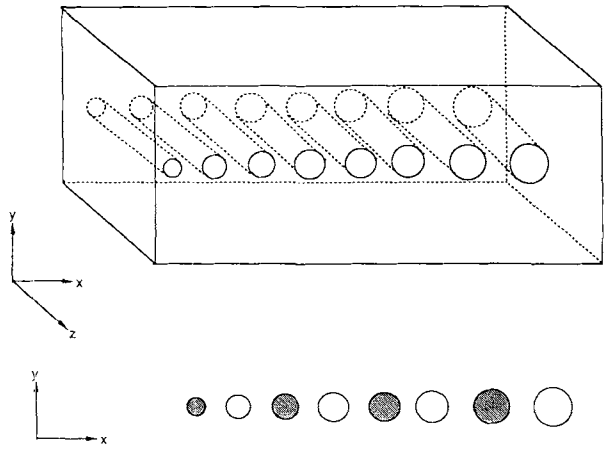

Figure 4. Schematic of first experimental phantom shows tubes of different sizes parallel to the z axis. The x, y, and z axes are the left-right, anteroposterior, and superoinferior directions, respectively, in the imager. A cross section in the x-y plane is also shown, with the shaded and unshaded tubes having opposite flow direction.

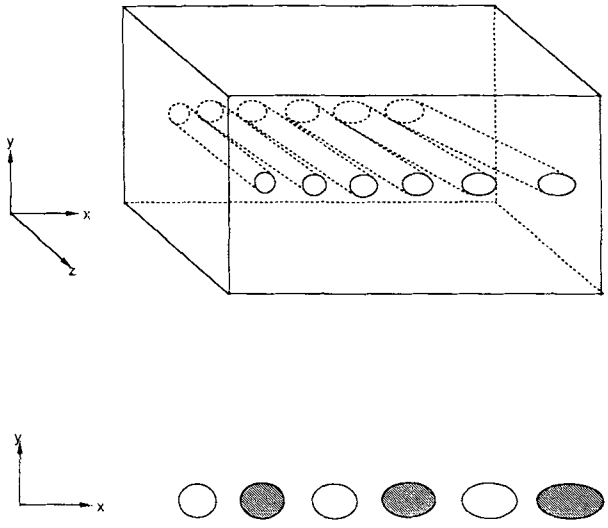

Figure 5. Schematic of second experimental phantom shows six tubes of identical size in the x-z plane, each tube at a different tilting angle relative to the z axis. A cross section in the x-y plane is also shown. The cross-sectional area increases as the tilting angle increases.

cos α, resulting in no change in the flow measurement. We note, however, that there will be a partial-volume effect due to section thickness that will affect measurement accuracy.

On the basis of the above discussion, we expect that the accuracy of the measured flow rate will depend on several factors, including (*a*) the relative signal intensity and volume fraction of flowing and stationary spins; (*b*) the flow type (eg, plug or laminar flow); (*c*) the relative size of the vessel and voxel grid; (*d*) the angulation between flow direction, velocity-encoding direction, and voxel grid; and (*e*) the relative positions of the vessel cross section and voxel grids.

• MATERIALS AND METHODS

Simulation Studies

Several simulation studies were conducted to demonstrate the effects of each factor on the phase-contrast flow measurement. For these studies, the saturation ratio (SR) is defined as the ratio between the signal magnitudes of stationary and flowing spins. Owing to time-of-flight effects, we assume that flowing spins have higher signal intensity per unit volume than stationary spins. Thus, SR—which depends on TR, TE, flip angle, T_1, T_2, and flow velocity—should be less than one. The relative position shift Δ is defined as the shift in position of the vessel relative to the voxel grid, normalized to the voxel length. As shown in Figure 2, the tessellation of the boundary voxels will change if the grid is shifted by only a fraction of a voxel and will not change if the grid is shifted by a multiple of the voxel size.

The velocities in each voxel are calculated by using Equation (15). The required values of Z_s, Z_{1v} (Eq [7]), and Z_{2v} (Eq [8]) are evaluated by numerical integration over the cross section of each voxel. The integration step sizes are subdivided until the tolerance of integration is better than 10^{-4}. The volume flow rate is the product of the voxel area and the sum of velocity values of all voxels covering the cross section of the vessel lumen, as described by Equation (17).

Table 1
Experimental MR Parameters for the First Phantom (Fig 4)

Parameter	Value
TR	33 msec
Flip angle	20°
Right-left resolution	256
Anteroposterior resolution	128
Superoinferior resolution	64
Resolution of low-pass filter	128, 64
Section orientation	Axial
Flow direction	Superoinferior
Velocity-encoding direction	Superoinferior
Field of view	24 cm
Section thickness	0.7 mm
Tube diameter	4.55, 5.75, 7.00, 8.15, 9.8, 9.8, 11.55, and 12.45 mm

In Vitro Experiments

In vitro phantom studies were performed to compare observed flow measurements with those predicted from simulation. The volume flow rate was measured as a function of spatial resolution for different tube sizes, flow rates, and relative positions. Volume flow rates were also measured as a function of section thickness for different tube angulation relative to the section plane.

Two gravity-driven flow phantoms consisting of tubes surrounded by air were constructed. The flow-

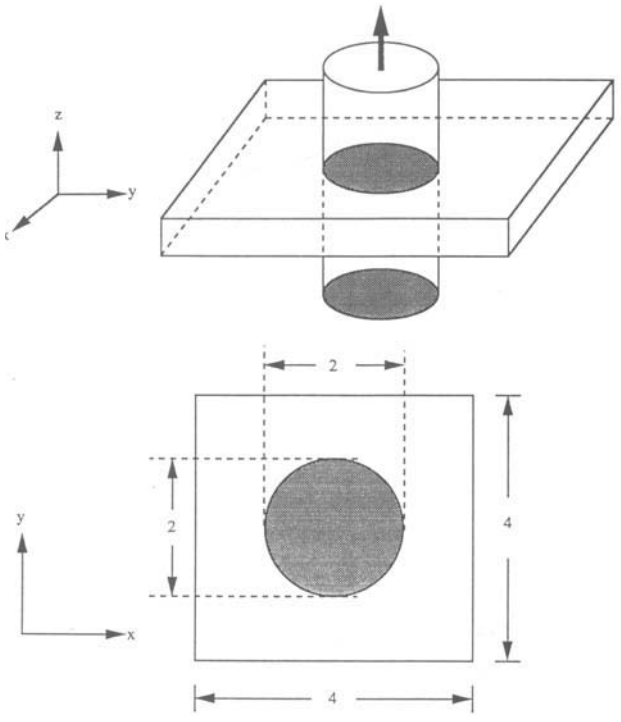

Figure 6. Schematic of first simulation model. The excitation plane is the x-y plane, and the flow and flow-encoding directions are along the z axis. The cross section in the x-y plane shows the tube with unit radius in a square with a width of 4 units.

ing water contained a few parts per million of copper sulfate to obtain a T1 of about 700 msec. In these experiments, stationary spins generate no signal and SR is zero. This is relevant to the situation in vivo, in which the magnetization of stationary tissues is highly saturated.

All the data were acquired on a 1.5-T Signa imaging system (GE Medical Systems, Milwaukee, Wis) with a shielded-gradient-coil subsystem. A three-dimensional phase-contrast pulse sequence was used (Fig 1), in which TE was made as short as possible to minimize the phase-dispersion effect. The three-dimensional phase-contrast method was used instead of the two-dimensional phase-contrast method to reduce image noise and to allow the study of a larger range of section thicknesses. Image processing was performed by using the C language on a Sun workstation (Sun Microsystems, Mountain View, Calif).

To eliminate large phase errors in voxels with no signal, we eliminated from analysis any voxel with a signal magnitude below an algorithm threshold. In these in vitro studies, the algorithm threshold was chosen to be twice the voxel standard deviation σ in the magnitude image. By varying the algorithm threshold, we also demonstrated the effect of eliminating the partially occupied boundary voxels.

Figure 4 shows the first phantom, consisting of tubes with inner diameters ranging from 4.55 to 12.45 mm. The experimental parameters are listed in Table 1. The tube orientations and velocity-encoding

Table 2
Experimental MR Parameters for the Second Phantom (Fig 5)

Parameter	Value
TR	33 msec
Flip angle	20°
Right-left resolution	256
Anteroposterior resolution	256
Superoinferior resolution	32
Section orientation	Axial
Flow direction relative to superoinferior direction	0°, 5°, 15°, 25°, 35°, and 50°
Velocity-encoding direction	Superoinferior
Field of view	24 cm
Section thickness	1.0, 2.0, 3.0, 4.0, and 5.0 mm
Tube diameter	6.35 mm

direction were set parallel to the main magnetic field. To prevent ghosting artifacts due to the small gradient amplitudes that result when large fields of view are used to increase voxel size, image spatial resolution was changed retrospectively by passing the complex image data through different Butterworth low-pass filters. For the three resolutions used, these filters were essentially equivalent to averaging blocks of one, four, and 16 image voxels together.

Figure 5 shows the second phantom, consisting of six tubes of equal diameter (6.35 mm). Each tube has a different angle relative to the direction of the main magnetic field, ranging from 0° to 50°. This experiment was designed to demonstrate the partial-volume effects that occur when the velocity-encoding direction is not parallel to the flow direction. The experimental parameters are listed in Table 2.

• RESULTS

Simulation Studies

The following computer simulations were performed to show the effect of the partial-volume effect on flow measurement accuracy. The volume flow rate was plotted as a function of resolution for different velocities (ie, different phase shifts), SRs, and relative position shifts. For comparison with the in vitro experiments, most of the simulation results were performed assuming SR to be zero. Simulation parameters are specified in the figure legends.

We first consider flow through the imaged section, as shown in Figure 6. For this simulation, the flowing spins are contained in the circle of unit radius. Outside the circle are stationary spins bounded in a square with a width of 4 units. The origin of coordinates is defined as the center of the square. The relative position between the tube and square is defined as the offset between the center of the tube and the center of the square divided by the voxel size. Because of the uniformity in the z direction, only variation in the x-y plane is considered.

Figure 7 shows the simulation results for the cases of plug and laminar flow.

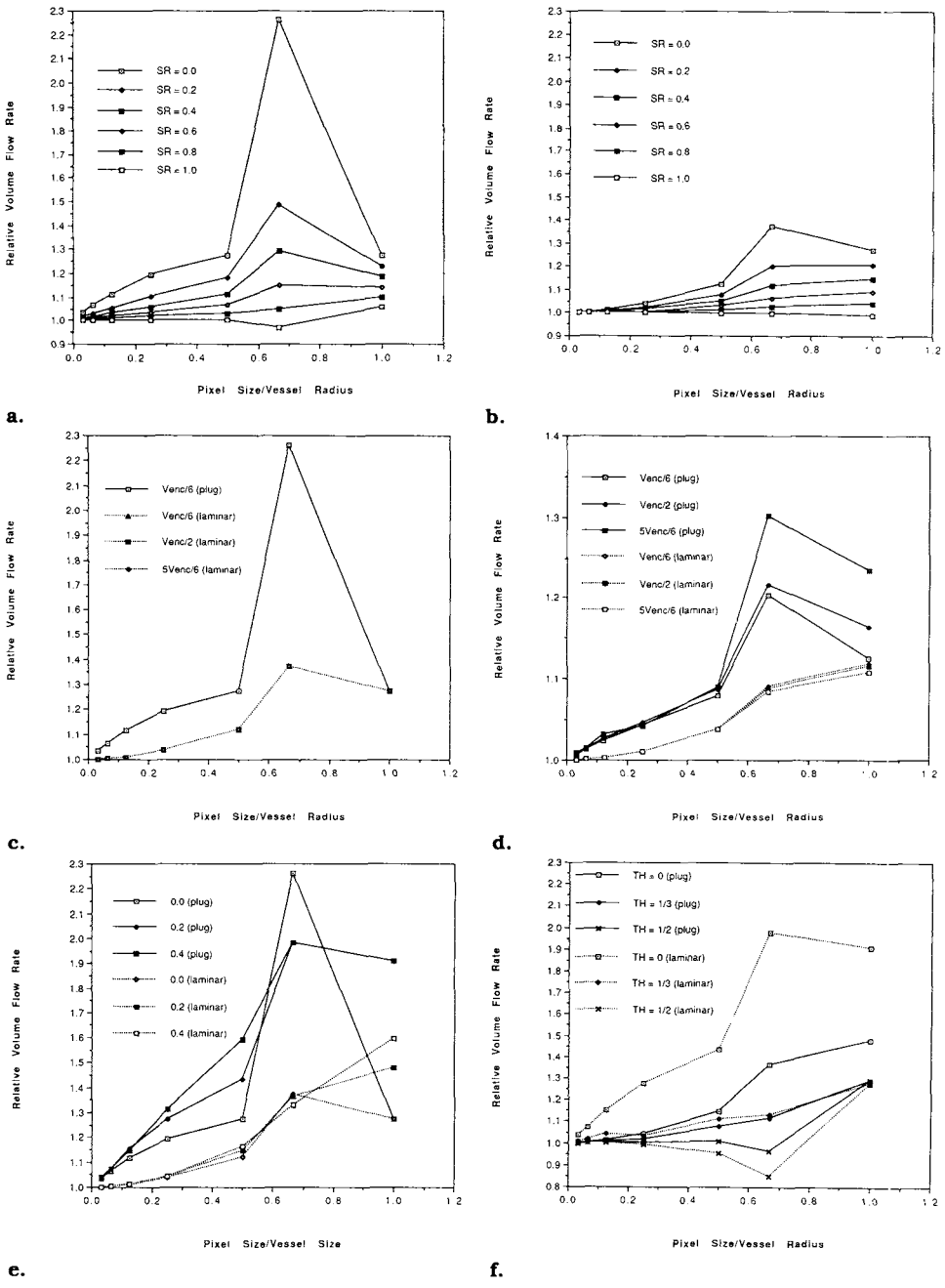

Figure 7. Simulation results in the case of plug and laminar flow. In **c–f**, the solid and dashed lines represent plug and laminar flow, respectively. Volume flow rate is plotted versus ratio of voxel size to vessel radius for **(a)** plug flow with $0.0 \leq SR \leq 1.0$, Δ (offset) = 0.2, and velocity = $v_{enc}/2$; **(b)** same conditions as in **a** except with laminar flow; **(c)** SR = 0.0, Δ = 0.2, velocity = $v_{enc}/6$ for plug flow and $v_{enc}/6$, $v_{enc}/2$, and $5v_{enc}/6$ for laminar flow; **(d)** SR = 0.5, Δ = 0.2, and velocity = $v_{enc}/6$, $v_{enc}/2$, and $5v_{enc}/6$; **(e)** SR = 0 Δ = 0.0, 0.2, and 0.4, and velocity = $v_{enc}/2$; and **(f)** thresholds (TH) = 0, ⅓, and ½ of the signal magnitude from a voxel totally occupied by flowing spins, SR = 0, velocity = $v_{enc}/2$, and Δ = 0.2.

By using the model shown in Figure 8, in which all the parameters are the same as for the model in Figure 6, we simulated volume flow rate as a function of the tilting angle α, with different section thicknesses, phase shifts, and SRs. Because of the angulation, there is a variation in flow velocity in the z direction that is not a two-dimensional problem as in the model in Figure 6. Also because of the angulation, the partial-volume effect from the shaded area illustrated in Figure 8c will affect the volume flow rate measurement. To minimize the computation time, we considered only the partial-volume effect in the image or section thickness (z) direction. We assumed infinite resolution in the x-y plane.

Figure 9 shows the relative volume flow rate for the case of plug flow as a function of the tilting angle for ratios of section thickness to vessel radius between 0.2 and 1.6. Because of the long computation time, the corresponding results for laminar flow were not computed. The results in Figure 9 do provide a general indication of flow-direction dependence that would exist for laminar flow.

In Vitro Experiments

Figure 10 is a plot of the relative volume flow rate as a function of the ratio between pixel size and tube radius. The results of the simulation of laminar flow in Figure 7e are overlaid on the graph.

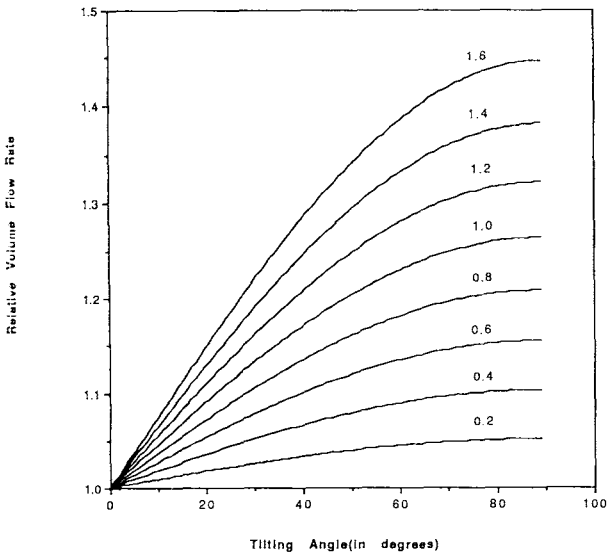

Figure 9. Relative volume flow rate in the case of plug flow plotted versus tilting angle for ratios of section thickness to vessel radius between 0.2 and 1.6.

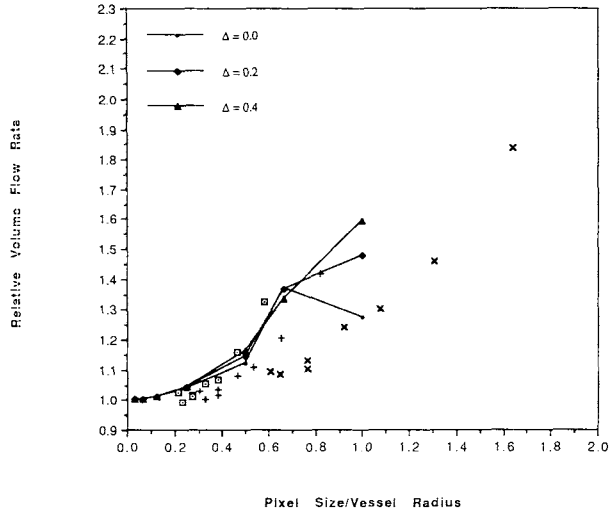

Figure 10. Relative volume flow rate plotted versus the ratio of pixel size to vessel radius. The results of the simulation of laminar flow in Figure 7e are overlaid on the graph. Volume flow rate measurements for the eight tube diameters listed in Table 1 were obtained from the original images (⊡) and from the same images processed with the Butterworth low-pass filter to 128 × 128 (+) and 64 × 64 (×) image resolutions.

Figure 11 is a plot of the relative volume flow rate as a function of the algorithm threshold for the 12.45- and 4.55-mm-diameter tubes. For the resolution used (24-cm field of view), the ratios between pixel size and tube radius are 0.2 and 0.6 for large and small tubes, respectively.

Figure 12 shows the relative volume flow rate as a function of tilting angle for different section thicknesses, using the experimental parameters given in Table 2.

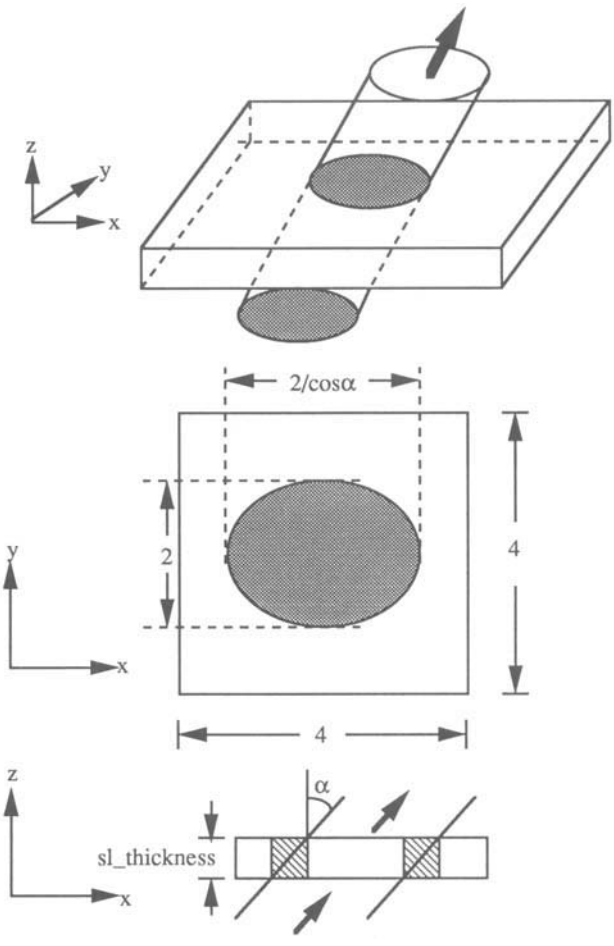

Figure 8. Schematic of second simulation model. The conditions are the same as for the first simulation model except that the flow direction is tilted an angle α away from the z axis in the x-z plane. Cross sections in the x-y and x-z planes are also shown. Shaded areas on the x-z plane cross section are the voxels that are partially occupied by stationary and flowing spins. *sl* = section.

• DISCUSSION

From all the figures for the simulation and in vitro studies, we can see that volume flow rate accuracy improves as resolution increases. They all explicitly show that the error in measured volume flow rate will be less than 10% if the ratio between voxel length and vessel radius is less than 0.5. We also see that the volume flow rate measurement fluctuates slightly as a function of several other parameters (velocity, phase shift, and threshold), but that these fluctuations decrease in magnitude as resolution improves. This implies that the accuracy of flow measurement could be improved by increasing the resolution alone, independent of the other parameters, which are usually unknown and uncontrollable. We also see that, in every case, the error observed in laminar flow is much less than that seen with plug flow.

As shown in Figure 7a and 7b, the flow rate measurement error is a strong function of SR and is greatly reduced when SR approaches 1. As pointed out in the Theory section, if there is no stationary sig-

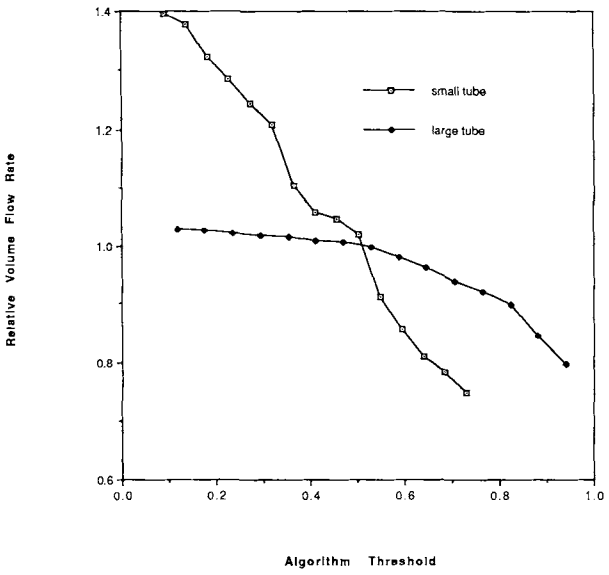

Figure 11. Volume flow rate plotted versus algorithm threshold for the 12.45- and the 4.55-mm-diameter tubes. Ratios of pixel size to vessel radius are 0.2 and 0.6 for the large tube and small tube, respectively.

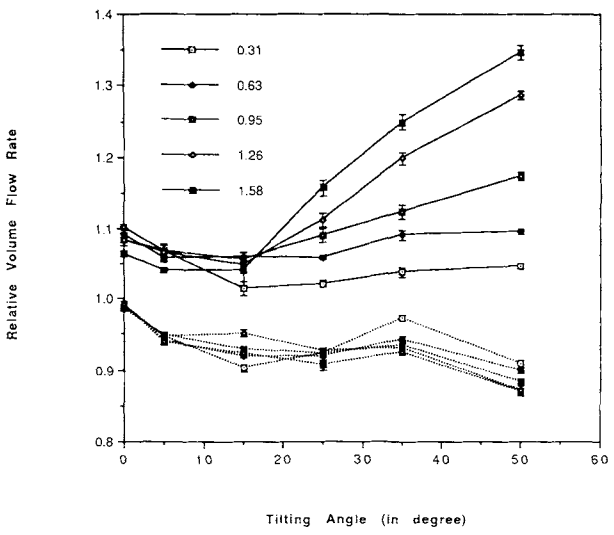

Figure 12. Volume flow rate plotted versus tilting angle at different section thicknesses, using the experimental parameters in Table 2. Solid and dotted lines represent thresholds of 0.1 and 0.5, respectively. The plots with the same symbol have the same section thickness. The numbers inside the graph represent the ratio of section thickness to tube radius. The standard deviation of the magnitude image (measured in air) was about 5% of the average signal magnitude of flowing spins.

nal and no velocity dispersion in a partially occupied voxel, the volume flow rate in the voxel will be overestimated because (*a*) the cross-sectional area is overestimated and (*b*) the velocity of flowing spins is accurately measured. As SR increases, the flow velocity will be underestimated. The underestimated velocity will tend to compensate for the overestimated cross-sectional area. The product of these two factors will approach the true volume flow rate. This effect is observed in Figure 7a and 7b, in which the accuracy of volume flow rate measurement improves as SR increases.

In Figure 7c and 7d, we see that the velocity dependence of the flow measurement also depends on SR. The simulation results shown in Figure 7c demonstrate the effect of intravoxel phase dispersion when there is no signal from stationary tissue (ie, SR = 0). Since there is no intravoxel phase dispersion in plug flow, the relative accuracy of volume flow rate measurement is independent of flow velocity (ie, the curves for all relative velocities would superimpose on the curve in Figure 7c. In the case of laminar flow, in which there is a dispersion of velocities within each voxel, the accuracy of the measured volume flow rate will depend on the actual flow rate. However, the laminar distribution of velocities within each voxel is relatively uniform, and even though an increase in velocity (or a decrease in v_{enc}) increases the phase dispersion within a given voxel, we have found that the velocity computed for the voxel obtained by using Equation (15) changes very little. We thus observe in Figure 7c that the effect of phase dispersion is negligible even for the low-resolution case in which four voxels cover the cross section of the vessel lumen.

In the case of a nonzero SR, the measured flow velocity (Eq [15]) will depend on the relative signals from flowing and stationary spins. As flow velocity changes, the measured relative volume flow rate (Eq [16]) will change for both laminar and plug flow (Fig 7d). For an SR of 0.5, the variation in volume flow rate with velocity is much less for laminar flow than for plug flow. The error in total volume flow rate results primarily from the volume flow rate errors in partially occupied boundary voxels. In laminar flow, the velocity gradually decreases from maximum velocity at the center of the vessel to zero at the boundary. The flow velocity is much lower near the boundary, and the volume flow rate of boundary voxels is less important. Contrary to laminar flow, plug flow has the same velocity across the vessel lumen, and the volume flow rate of the boundary voxels is important.

The relative effect of the edge voxels is demonstrated in Figure 7f, in which the measured volume flow rate is plotted against algorithm thresholds of 0 (top plot) and one-third (bottom plot) of the signal magnitude of a voxel fully occupied with flowing spins. This figure shows that increasing the threshold causes a much greater change in the case of plug flow than in laminar flow. That the plug flow measurement is much more sensitive to the choice of threshold again demonstrates that the partial-volume effect is much greater for plug flow than for laminar flow.

From a set of measurements made on the same in vitro image (Fig 11), we see that the volume flow rate changes slightly with threshold for the large tube and changes substantially with threshold for the small tube. The ratio between the number of partially occupied and fully occupied voxels is larger in the small tube than in the large one, and inclusion and exclusion of even a small number of partially occupied vox-

els will have a substantial effect on the flow measurement in the small tube. So the accuracy of volume flow measurements will be sensitive to the selection of threshold in small vessels and in low-resolution flow measurements. The relative volume flow rate approaches 1 at an algorithm threshold of about 0.5. This result is consistent with the observation of Pelc et al (9), who suggested the use of a threshold at the isointensity contour midway between the intraluminal signal and the background signal. We believe that the algorithm threshold excludes only partially occupied voxels when it is less than 0.5 and starts to exclude fully occupied slow-flow voxels when it increases.

In Figure 9, which plots the dependence of the volume flow rate measurement on tilting angle and section thickness, we see that the accuracy improves with reduction in the partial-volume effect as the tilting angle and/or section thickness decrease. Had it been possible to consider finite resolution in the x-y plane, we would expect that the flow measurement error would have been even larger because of the partial-volume effect in the x-y plane. Figure 12 provides in vitro experimental confirmation that the volume flow rate measurement error increases with increasing section thickness and tilting angle. The deviation of these experimental measurements from the simulation results of Figure 9 occurs primarily at small tilting angles and thin section thicknesses, at which in-plane partial-volume effects not simulated in Figure 9 begin to dominate.

The accuracy of flow measurement is subject to many factors, as described above. If vessel orientation is known a priori, we can select the section- and flow-encoding directions to be parallel to the vessel to minimize partial-volume effects. If several vessels with different orientations are studied, the flow in large vessels with small tilting angles relative to the flow-encoding direction will be measured most accurately.

There are several other potential sources of error that we did not study. These include the effects of eddy currents, phase or frequency artifacts, pulsatile flow, and velocity aliasing. Eddy currents—which can be a major concern in phase-contrast flow measurements (10)—do not appear to be a problem because of our use of a shielded-gradient-coil subsystem.

Oblique flow can cause a misregistration artifact because the different spatial coordinates are encoded at different times (11,12). With laminar flow, spins at different positions will be shifted by different amounts. This will cause spins to appear to overlap and produce regions of signal enhancement and signal void. If the flow is fast enough, the vessel structure may seem to extend outside of the actual vessel lumen. Our initial estimate, based on the velocity of flow, the different encoding times for the different axes, and the size of tubes, was that this artifact would not be a problem in our studies. Further investigation is being conducted to study the effect of the misregistration artifact on flow measurement.

For in vivo imaging, pulsatile flow that includes higher orders of motion (13,14) will create ghosts in the phase-encoding direction, blur the images, and affect flow measurement. To reduce this artifact, several techniques such as (*a*) higher-order moment nulling, (*b*) phase-encoding reordering, (*c*) cardiac gating, and (*d*) half-Fourier imaging could be implemented.

• CONCLUSION

We have analyzed the accuracy of phase-contrast volume flow measurements. Both the simulation and in vitro studies demonstrate that measurement accuracy depends strongly on spatial resolution and improves as voxel size is reduced relative to vessel dimensions. When the encoding direction is parallel to the flow direction, at least 16 isotropic voxels must cover the cross section of the vessel lumen to achieve a flow measurement accuracy within 10% of the true value. If the encoding direction is not parallel to the flow direction, the resolution in all three directions must increase accordingly to maintain accuracy. When resolution is limited, accuracy depends strongly on the relative signal intensity of stationary tissue. The simulations also show that laminar flow can be measured more accurately than plug flow at the same resolution. Because there is no velocity dispersion in plug flow and because the threshold dependence in the in vitro study was greater for small than for large tubes, we conclude that the partial-volume effect is more important than the phase-dispersion effect in quantitative flow measurement accuracy. ●

Acknowledgment: The authors thank Matt Bernstein, PhD, for useful discussions and Dr Richard Robb of the Mayo Foundation for the use of the Analyze software package.

References

1. Axel L. Blood flow effects in magnetic resonance imaging. AJR 1984; 143:1157–1166.
2. Singer JR. Blood flow rate by nuclear magnetic resonance imaging. Science 1959; 130:1652–1653.
3. Dumoulin CL, Hart HR. Magnetic resonance angiography. Radiology 1986; 161:717–720.
4. Dumoulin CL, Souza SP, Walker MF, Wagle W. Three dimensional phase contrast angiography. Magn Reson Med 1989; 9:139–149.
5. Moran PR, Moran RA, Karstaedt N. Verification and evaluation of internal flow and motion. Radiology 1985; 154: 433–441.
6. Bryant DJ, Payne JA, Firmin DN, Longmore DB. Measurement of flow with NMR imaging using a gradient pulse and phase difference technique. J Comput Assist Tomogr 1984; 8:588–593.
7. Pelc NJ, Bernstein MA, Shimakawa A, Glover GH. Encoding strategies for three-direction phase-contrast MR imaging of flow. JMRI 1991; 1:405–413.
8. Hausmann R, Lewin JS, Laub G. Phase-contrast MR angiography with reduced acquisition time: new concepts in sequence design. JMRI 1991; 1:415–422.
9. Pelc NJ, Sommer FG, Enzmann DR, Pelc LR, Glover GH. Accuracy and precision of phase-contrast MR flow measurements (abstr). Radiology 1991; 181(P):189.
10. Ahn CD, Cho ZH. Analysis of eddy currents in nuclear magnetic resonance imaging. Magn Reson Med 1991; 17: 149–163.
11. Nishimura DM, Jackson JI, Pauly JM. On the nature and reduction of displacement artifact in flow images. Magn Reson Med 1991; 22:481–492.
12. Larson TC, Kelly WM, Ehman RL, Wehrli FW. Spatial misregistration of vascular flow during MR imaging of CNS: cause and clinical significance. AJR 1990; 155:1117–1124.
13. Wood ML, Henkelman RM. MR image artifacts from periodic motion. Med Phys 1985; 12:143–151.
14. Perman WH, Moran PR, Moran RA, Bernstein MA. Artifacts from pulsatile flow in MR imaging. J Comput Assist Tomogr 1986; 10:473–483.